Received: 7 May 2019 | Revised: 5 October 2019 | Accepted: 7 October 2019

DOI: 10.1111/jmg.12512

ORIGINAL ARTICLE

Journal of METAMORPHIC GEOLOGY WILEY

Calibration of oxygen isotope fractionation and calcite-corundum thermometry in emery at Naxos, Greece

Rachelle B. Turnier[1] | **Yaron Katzir**[2] | **Kouki Kitajima**[1] | **Ian J. Orland**[1] | **Michael J. Spicuzza**[1] | **John W. Valley**[1]

[1]Department of Geoscience, University of Wisconsin, Madison, Wisconsin

[2]Department of Geological and Environmental Sciences, Ben Gurion University of the Negev, Be'er Sheva, Israel

Correspondence
Rachelle B. Turnier, Department of Geoscience, University of Wisconsin-Madison, Madison, WI 53706, USA.
Email: turnier@wisc.edu

Funding information
National Science Foundation, Grant/Award Number: EAR-1525336, EAR-1355590 and 1658823; UW-Madison

Handling Editor: Donna L. Whitney

Abstract

Corundum (Crn), including sapphire, occurs in emery pods surrounded by marble on the island of Naxos, Greece. The emery formed from bauxite deposited in karst that was metamorphosed to 400–700°C at 20–15 Ma. Many of these rocks initially appeared well suited for refractory accessory mineral (RAM) thermometry, which uses oxygen isotope fractionation between a RAM – corundum – and a modally dominant phase with faster diffusion of oxygen – calcite (Cc) – to determine peak metamorphic temperatures. However, previous attempts at oxygen isotope thermometry were confounded by highly variable fractionations ($\Delta^{18}O$) measured at mm-scale and the uncertain calibration of $\Delta^{18}O$(Cc-Crn) versus temperature. Secondary ion mass spectrometry (SIMS) permits in situ analysis of $\delta^{18}O$ in corundum and calcite at the 10-μm scale in adjacent grains where textures suggest peak metamorphic equilibrium was attained. SIMS analyses of adjacent mineral pairs in eight rocks yield values of Δ(Cc-Crn) that systematically decrease from 7.2 to 2.9‰ at higher metamorphic grade. Pairing these data with independent temperature estimates from mineral isograds yields an empirical calibration of $1{,}000\ \ln\alpha(\text{Cc-Crn}) = 2.72 \pm 0.3 \times 10^6/T^2$ (T in K). The new fractionations (2.7‰ at 1,000 K) are significantly smaller than those calculated from the modified increment method (6.5‰ at 1,000 K; Zheng, Geochimica et Cosmochimica Acta, 1991, 55:2299–2307; Zheng, Mineral Mag, 1994, 58A:1000–1001), which yield unreasonably high temperatures of 630 to 1,140°C when applied to the new Naxos data. The new calibration of Δ(Cc-Crn) can be combined with published fractionations to calculate A-factors for corundum versus a range of 14 other minerals. These new fractionation factors can be used for thermometry or to constrain the genesis of corundum. A compilation of gem corundum $\delta^{18}O$ values shows that many igneous sapphires, including important deposits of basalt-associated sapphire, are mildly elevated in $\delta^{18}O$ relative to the calculated range in equilibrium with mantle values (4.4–5.7‰) and formed from evolved magmas.

KEYWORDS

calcite, corundum, oxygen isotope fractionation, SIMS, thermometry

1 | INTRODUCTION

Mineral-corundum fractionation factors have many applications, one of which is investigating sapphire genesis. Most gem sapphires are mined from placer deposits, but when they are found in igneous host rocks, textural and chemical evidence often indicates they are xenocrysts and their genesis is uncertain (Giuliani, Ohnenstetter, Fallick, Groat, & Fagan, 2014). Are they igneous or metamorphic? Did they crystallize in the deep crust or mantle, from primitive or evolved magmas that have undergone crustal interactions? Evaluating oxygen isotope fractionation between coexisting minerals is a useful technique for understanding mineral paragenesis and crystallization temperature.

The fractionation of $^{18}O/^{16}O$ among mineral pairs equilibrated at a given temperature is commonly used as a thermometer (Hoefs, 2018; O'Neil, 1986; Valley, 2001). This relation can be represented by a linear, one-coefficient equation:

$$1000\ \ln\alpha\,(a-b)=\frac{A\,(a-b)\times 10^6}{T^2}, \tag{1}$$

where $\alpha(a\text{-}b)$ is the fractionation factor, A(a-b) is a constant referred to as the A-factor, T is temperature (in Kelvin), and a and b are the two minerals (for mineral abbreviations used in this study, see Table 1). Values of 1,000 lnα(a-b) can be approximated by $\delta^{18}O(a)$ - $\delta^{18}O(b)$ (= $\Delta^{18}O(a\text{-}b)$). Thus, equilibration temperature can be calculated from the oxygen isotope ratios of two minerals if they preserve isotope equilibrium and the A-factor is known.

Calcite-corundum oxygen isotope fractionation has been estimated from modified increment method calculations of corundum-water and calcite-water fractionation with three coefficients (Zheng, 1991, 1994), which equates to:

$$1000\ \ln\alpha\,(\mathrm{Cc}-\mathrm{Crn})=\left(\frac{1.77\times 10^6}{T^2}+\frac{9.05\times 10^3}{T}-4.34\right). \tag{2}$$

At 1,000 K (727°C), Equation 2 gives $\Delta^{18}O$(Cc-Crn) = 6.5‰, and Equation 1 can then be solved to show that this value equates to the A-factor (A(Cc-Crn)). However, the fractionations from Equation 2 have been questioned as yielding temperatures that are unreasonably high (Yui, Zaw, & Wu, 2008). Likewise, Fallick et al. (2019) evaluate the modified increment fractionation factors for $\Delta^{18}O$(Cc-spinel) from marbles and also conclude that the fractionation factors yield unreasonably high metamorphic temperatures. Since there is no experimental calibration of oxygen isotope fractionation in corundum, the approach taken here is to calibrate 1,000 lnα(Cc-Crn) using measured data in comparison with isograd temperatures in metamorphic calcite-corundum rocks.

Metamorphic minerals are often zoned or heterogeneous in $\delta^{18}O$ (Ferry, Kitajima, Strickland, & Valley, 2014) reflecting a range of prograde and retrograde processes. Minerals with slow rates of oxygen diffusion can be homogeneous or preserve growth zoning if crystallized below their Dodson closure temperature. Minerals with faster diffusion can be reset by exchange during cooling, which frequently leads to retrograde zoning patterns (Eiler, Baumgartner, & Valley, 1992; Eiler, Valley, & Baumgartner, 1993). Under ideal conditions, the effects of diffusion, which are deleterious for thermometry, can be avoided by analysis of a 'refractory' mineral with slow diffusion that is modally minor and crystallized in a rock dominated by a mineral with fast diffusion (Valley, 2001). Such refractory accessory mineral (RAM) thermometry can be applied to accessory minerals such as corundum, aluminosilicates, magnetite, pyroxene or garnet in marble, quartzite or anorthosite for $\delta^{18}O$; or graphite in marble for $\delta^{13}C$.

In appropriate rocks, RAM thermometry can be used without calculating diffusion effects because the fast-exchanging mineral is modally abundant. In the absence of fluid flow, it does not change significantly in $\delta^{18}O$ due to mass balance. The slow-exchanging accessory mineral preserves its $\delta^{18}O$ value and thus the $\Delta^{18}O$ from crystallization. Although RAM thermometry has been successfully applied in a range of rocks at mm- to cm-scale using bulk analysis techniques (Kitchen & Valley, 1995; Putlitz, Valley, Matthews, & Katzir, 2002; Valley, 2001), the effects of overprinting events can be confounding. More recently, it has become possible to evaluate such formerly cryptic effects by employing in situ analysis at μm-scale by secondary ion mass spectrometry (SIMS; Bowman, Valley, & Kita, 2009; Errico, Barnes, Strickland, & Valley, 2013; Ferry et al., 2014; Ferry, Ushikubo, Kita, & Valley, 2010; Gordon et al., 2012; Page, Essene, Mukasa, & Valley, 2014; Quinn, Kitajima, Nakashima, Spicuzza, & Valley, 2017; Russell et al., 2013; Valley, 2001; Valley & Kita, 2009; Vielzeuf, Champenois, Valley, Brunet, & Devidal, 2005).

Corundum and calcite in the metamorphosed karst bauxite emery from Naxos, Greece (Figure 1) provide a promising setting for RAM thermometry, or alternatively, for empirical calibration of the calcite-corundum A-factor. The samples in this study approximate bi-mineral assemblages that are suitable for RAM thermometry. SIMS measurements were made on a local scale in domains of ~500 × 500 μm. The metamorphic temperatures have been independently determined by mineral isograds to increase from 400°C in the SE to 700°C at the migmatite dome in the NW part of the island (Figure 1; Feenstra & Wunder, 2002). Details of mineral isograds are discussed in Section 2.

In an earlier attempt to calibrate the A-factor using rocks from Naxos, oxygen isotope ratios were measured in bulk mineral separates from volumes of one cubic centimetre or larger by laser fluorination (corundum; Table S1) and acid solution (calcite; Table S2) techniques (Katzir & Valley,

TABLE 1 Summary of data for samples 1–8, including sample name, mineralogy, temperature interpolated from isograds (Figure 1), SIMS average $\delta^{18}O$ and 2SD of calcite and corundum values for close mineral pairs, fractionation and propagated analytical 2SD, the average 2SD of fractionation within a sample, and latitude and longitude. The calcite-corundum fractionation, Δ(Cc-Crn), for each sample is an average of within-sample fractionations from close calcite-corundum pairs. Sample numbers correspond to locations shown in Figure 1. Mica refers to margarite, paragonite, or muscovite and 'oxides' include Fe oxide, Ti oxide, or Fe-Ti oxide. The data for close calcite-corundum pairs and the propagated analytical uncertainty are summarized in Table S3.2

Sample no. (Figure 1)	Sample name	Minerals	Isograd T (°C)	$\delta^{18}O$(Cc) Avg. ± 2*SD* (‰) VSMOW	$\delta^{18}O$(Crn) Avg. ± 2*SD* (‰) VSMOW	Δ(Cc-Crn) ± 2*SD* Prop. (‰)	Within- Sample 2*SD* Δ(Cc-Crn) (‰)	Latitude	Longitude
1	NM-1-368	Cc, Crn, mica, oxides, An	593	25.3 ± 0.48 (n = 10)	21.9 ± 0.69 (n = 10)	3.38 ± 0.37	0.67	37°6′42.00″ N	25°32′24.48″ E
2	NL-4-351	Cc, Crn, mica, oxides, Czo/Ep	577	22.0 ± 0.86 (n = 8)	18.9 ± 0.99 (n = 8)	3.08 ± 0.56	1.57	37°7′56.16″ N	25°33′49.05″ E
3	NL-7-358	Cc, Crn, mica, oxides, Tur	574	24.5 ± 0.58 (n = 10)	20.7 ± 0.52 (n = 10)	3.77 ± 0.30	0.33	37°8′3.91″ N	25°34′2.73″ E
4	NL-3-40Aa	Cc, Crn, mica, oxides, Ap	570	20.6 ± 0.72 (n = 21)	17.7 ± 0.72 (n = 21)	2.93 ± 0.41	0.95	37°7′28.98″ N	25°33′55.20″ E
5	NL-3-40Ba	Cc, Crn, mica, oxides	570	21.0 ± 0.72 (n = 24)	17.7 ± 0.78 (n = 24)	3.28 ± 0.38	1.30	37°7′28.98″ N	25°33′55.20″ E
6	NL-8-359	Cc, Crn, mica, oxides, Czo/Ep	568	22.3 ± 0.31 (n = 12)	18.7 ± 0.53 (n = 12)	3.67 ± 0.43	0.52	37°7′39.94″ N	25°33′53.75″ E
7	NOA-381	Cc, Crn, mica, oxides, Dsp	425	26.0 ± 0.72 (n = 15)	18.75 ± 0.61 (n = 15)	7.20 ± 0.37	0.64	36°56′44.20″ N	25°25′34.69″ E
8	NZ-3-434	Cc, Crn, mica, oxides, Czo/Ep	424	22.3 ± 0.36 (n = 9)	15.9 ± 1.15 (n = 10)	6.33 ± 0.33	1.21	36°58′42.99″ N	25°28′26.04″ E

Note: Abbreviations: Ab, albite; Alm, almandine; An, anorthite; Ap, apatite; Cc, calcite; Crn, corundum; Czo, clinozoisite; Di, diopside; Dsp, diaspore; Ep, epidote; Fo, forsterite; Gr, grossular; Ky, kyanite; Mrg, margarite; Mt, magnetite; Pg, paragonite; Prv, perovskite; Qz, quartz; Ru, rutile; Sp, spinel ($MgAl_2O_4$); Ttn, titanite; Tur, tourmaline; Zrc, zircon.

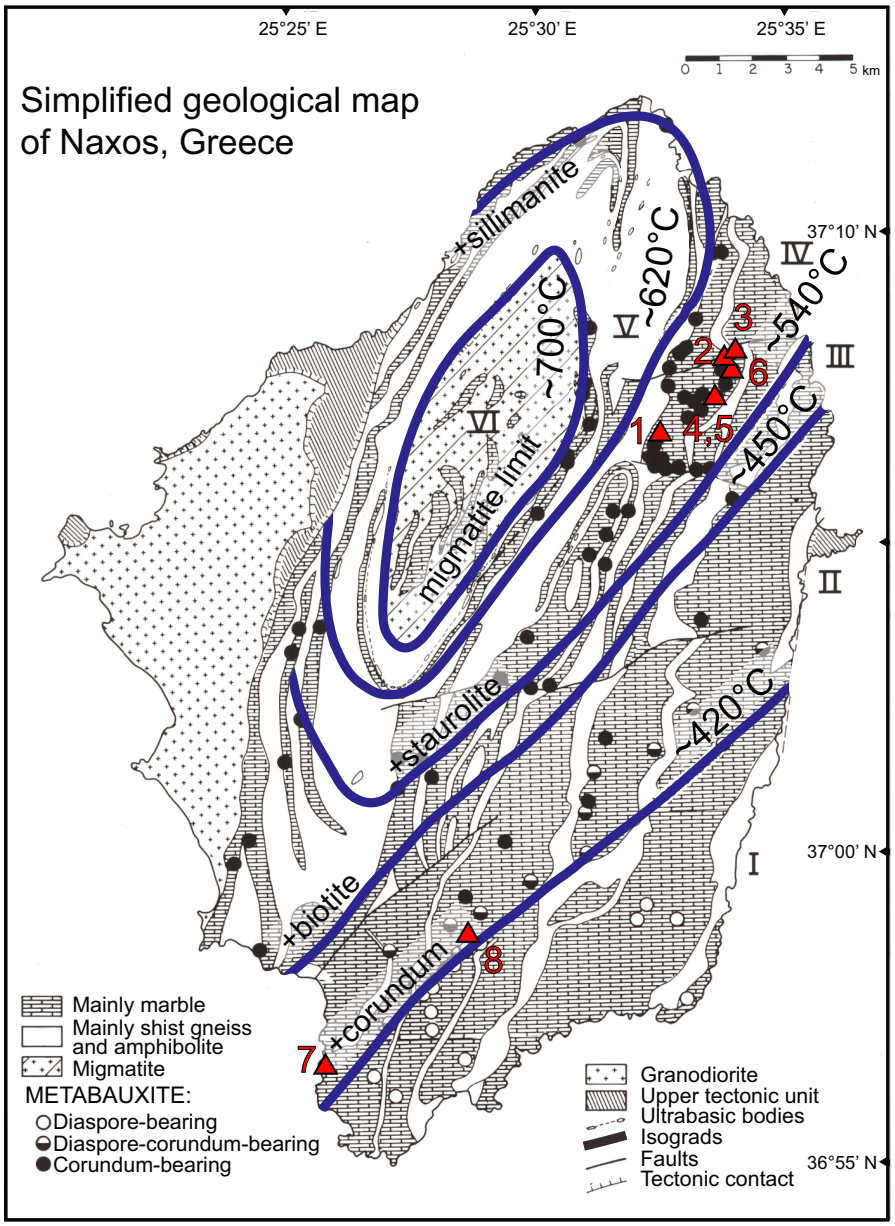

FIGURE 1 Simplified geological map of Naxos, Greece, showing isograds and temperatures for M2 metamorphism, modified from Feenstra and Wunder (2002). Black and half-filled dots are locations of corundum. Red triangles and accompanying numbers denote the location of samples collected and analysed for this study

2001). However, these analyses homogenized mineral grains that might have been zoned or contained inclusions and veins. Fractionations, $\Delta^{18}O$(Cc-Crn), ranged by over 10‰ from −2.0 to +8.4‰ in 17 rocks (Table S1.1 in Appendix S1). These fractionations include reversals from negative to positive and are not consistent with sample temperature estimates of ~420–590°C, based on mineral isograds for M2 metamorphism (see Section 2) of corundum-bearing rocks across Naxos.

In the current study, we analysed samples using SIMS (10 μm spots) in order to test for isotopic zonation and alteration that would impact the determination of equilibrium $\delta^{18}O$ values of calcite and corundum. Samples were imaged by SEM-based cathodoluminescence (CL), secondary electrons (SE), and backscattered electrons (BSE) to guide in situ measurements. The textural and isotopic complexity of the Naxos emery samples (Figures 2–5) indicate the need to make oxygen isotope analyses in situ by SIMS in order to avoid micro-inclusions, prograde- and retrograde-growth zones, and secondary minerals like vein calcite that do not relate to the high-temperature equilibrium attained during metamorphism.

Microanalysis by SIMS allows evaluation of possible variability and disequilibrium of $\delta^{18}O$ within volumes smaller than analysed at the mm-scale. Analyses of close pairs of corundum and calcite grains are compared with the isograd temperatures in order to empirically calibrate the A-factor in Equation 1. From published data for calcite-mineral fractionation factors (Chacko, Cole, & Horita, 2001; Valley, 2003), the A-factor for corundum versus other minerals can then be calculated. We apply these new calibrations to explore the genesis of other corundum deposits, especially basalt-hosted sapphires.

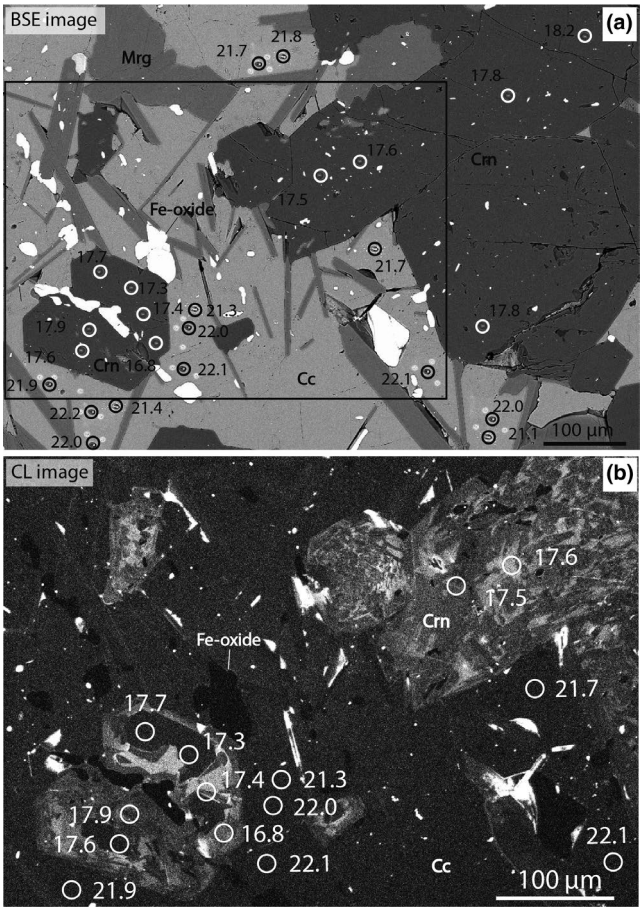

FIGURE 2 Backscattered electrons (BSE) and cathodoluminescence (CL) images for high-temperature sample 5 showing $\delta^{18}O$ (‰ VSMOW) measured in situ by SIMS in corundum and calcite from emery (Naxos, Greece). Black box in (a) denotes location of CL image in (b). CL and SE images were overlain to emphasize grain boundaries. Images show dispersed inclusions of mostly Fe oxides, which are bright by BSE. By SIMS it is possible to avoid these phases and obtain $\delta^{18}O$ measurements for close pairs of corundum and calcite. Circles and adjacent values present the location of SIMS pits and corresponding $\delta^{18}O$. Circles are larger than analytical spot size

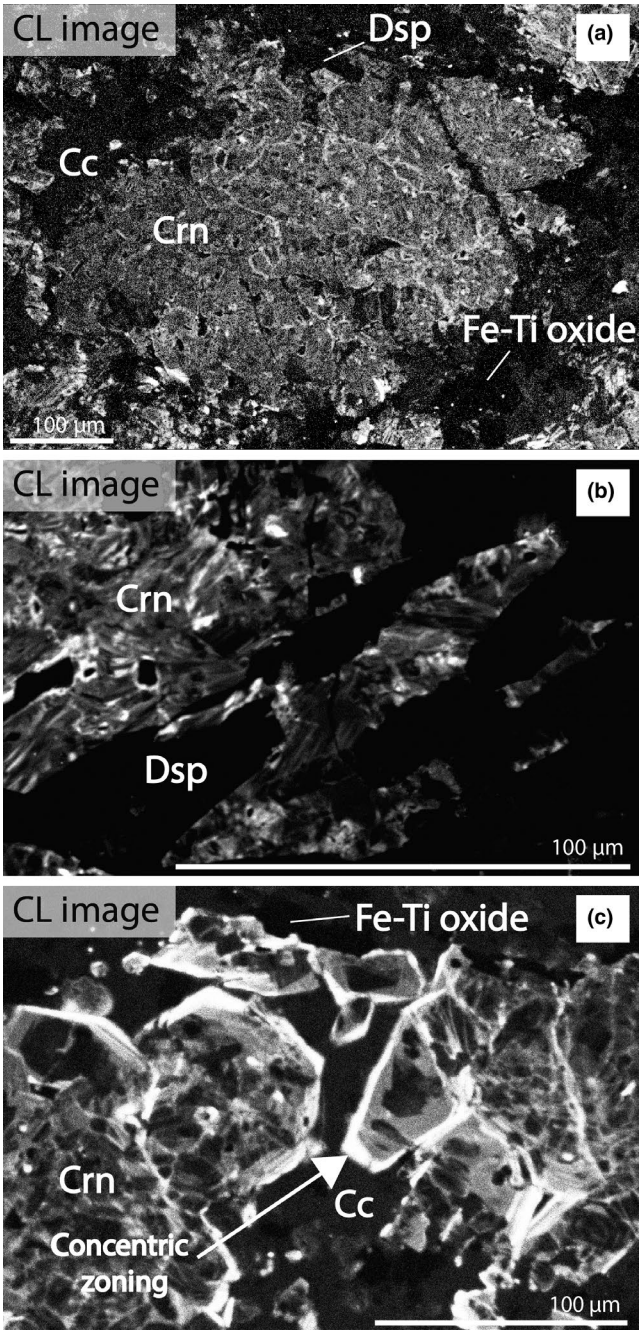

FIGURE 3 Image of representative cathodoluminescence textures in low-temperature samples of emery (Naxos, Greece). Images (a) and (b) are from sample 7, (c) is sample 8. Panel (c) shows complex interior textures of corundum grains in addition to later concentric zones mantling the exterior of the grain

2 | NAXOS GEOLOGY AND SAMPLE SELECTION

The island of Naxos, Greece, consists of mostly schist, gneiss, and marble (the main host of metabauxite lenses). Sediments were originally deposited in a shallow-sea environment (Aydoğan & Moazzen, 2012) that was later exposed as karst topography to subaerial weathering and lateritic infilling. Naxos has experienced two major metamorphic events that turned the karst bauxite to marble and emery: M1, an Eocene blueschist- to eclogite-facies event, and M2, a Miocene greenschist- to amphibolite-facies event (Avigad, 1998; Bolhar, Ring, & Ireland, 2017; Keay, Lister, & Buick, 2001; Martin, Duchéne, Deloule, & Vanderheaghe, 2006; Wijbrans & McDougall, 1988). The M2 metamorphism overprinted M1 assemblages and resulted in a metamorphic thermal gradient on the island of Naxos that is reflected in a series of mineral isograds.

From low- to high-grade metamorphism, the isograds divide the rocks on Naxos into a series of metamorphic zones (zones I–VI, Figure 1), which are defined based on the characteristic mineral assemblages in the pelitic schists and

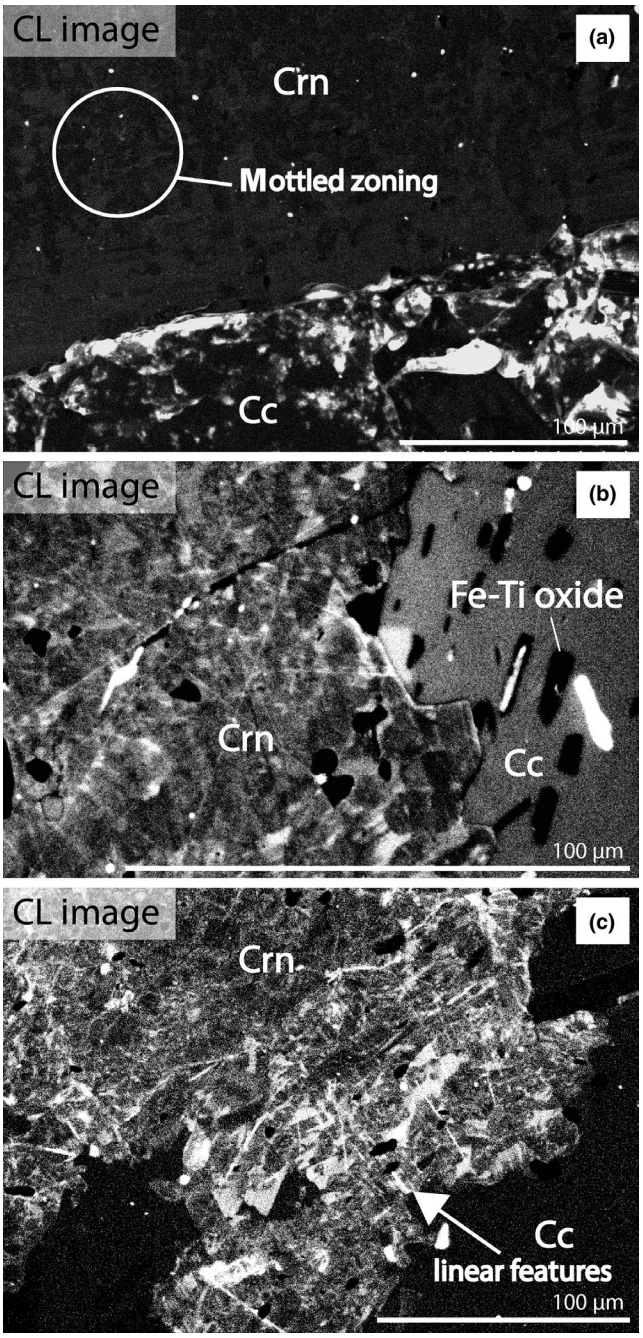

FIGURE 4 Images of cathodoluminescence (CL) textures seen in high-temperature samples of emery (Naxos, Greece). Image (a) is from sample 2, (b) is from sample 6, and (c) is from sample 4. Panels (a) and (b) show mottled dark and slightly brighter CL textures, while (c) shows some mottled zoning along with linear features

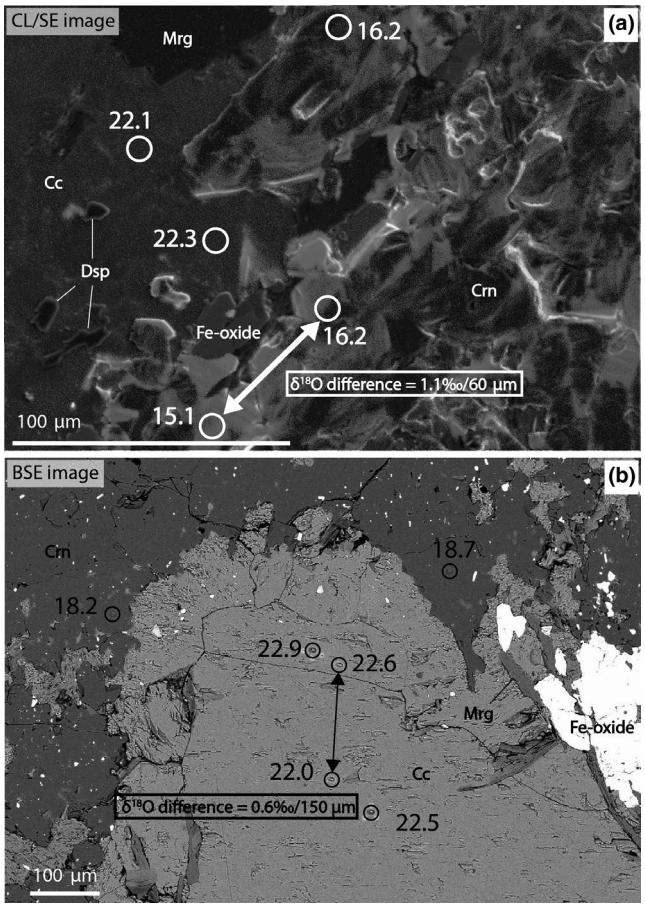

FIGURE 5 Backscattered electrons (BSE) and cathodoluminescence (CL) images showing largest measured isotopic differences in corundum (panel a; sample 8) and calcite (panel b; sample 2) from emery (Naxos, Greece). Circles mark locations of SIMS pits, which are smaller and visible within the circle; adjacent numbers are $\delta^{18}O$ (‰ VSMOW). Note: maximum isotopic difference shown in calcite (panel b) is statistically insignificant

metabauxites. Pressures for M2 on Naxos range from 6 to 8 kbar (Buick, 1988; Voudouris et al., 2019) and isograd temperatures range from 420 to 700 ± 50°C (Buick, 1988; Buick & Holland, 1989). Mineral isograds were first mapped by Schuiling and Oosterom (1967), and then refined by Jansen and Schuiling (1976) and Buick (1988). Isograd index minerals were mapped based on field observations and verified in the lab with thin sections and X-ray diffraction (Jansen, 1977). Isograd temperatures are consistent with those obtained by garnet-biotite exchange thermometry by Duchêne, Aïssa, and Vanderhaeghe (2006). This information is summarized here in terms of the metabauxite mineral assemblages from each zone, the occurrence of index minerals, and the characteristic reactions for each mineral isograd separating the zones.

Zone I is the diaspore-chloritoid zone, where metabauxites contain diaspore, chloritoid, Fe-Ti oxides, rutile ± calcite (in the outer rims and, locally, central parts of the metabauxite bodies; Feenstra, 1985). The pelitic schists have a greenschist-facies assemblage of albite–quartz–chlorite–sericite (Jansen & Schuiling, 1976). The first isograd, corundum-in, is defined by the reaction of diaspore to corundum and water; it was mapped based on the appearance of corundum in 25 metabauxite occurrences (Jansen & Schuiling, 1976). On Naxos, this reaction occurs at ~6–7 kbar and 420°C (Feenstra & Wunder, 2002).

TABLE 2 Modal abundances of minerals determined by SEM in 1 mm domains analysed by SIMS from samples 1–8

Sample #:	1	2	3	4	5	6	7	8
Phase	**Modal (%)**	**Modal (%)**	**Modal (%)**	**Modal (%)**	**Modal (%)**	**Modal (%)**	**Modal (%)**	**Modal (%)**
Cc	68	28	78	52	67	66	26	32
Crn	12	50	9	15	12	14	46	42
Mica	5	14	4	23	15	10	10	6
Oxides	2	5	1	6	5	5	6	11
Tur	—	—	8	—	—	—	—	—
An	13	—	—	—	—	—	—	—
Czo	—	3	—	—	—	4	—	9
Ap	—	—	—	3	—	—	—	—
Dsp	—	—	—	—	—	—	12	—

The corundum-in isograd marks the beginning of zone II, the chlorite-sericite zone. Metabauxites in zone II contain mainly corundum–chloritoid–Fe oxide (Feenstra, 1985), but also have calcite near marble-metabauxite contacts (samples 7 and 8, this study). Minerals in the schists are similar to those in zone I schists (Jansen & Schuiling, 1976).

The next isograd, biotite-in, is mapped based on 30 field observations of biotite in pelites (Jansen & Schuiling, 1976). The biotite-in isograd marks the beginning of zone III: the biotite-chloritoid zone. Biotite may be formed by the breakdown of chlorite and muscovite (Schuiling & Oosterom, 1967). This occurs at ~450°C on Naxos (Baker & Matthews, 1994; Jansen, 1977). Biotite was not detected in the zone III metabauxites (Feenstra, 1985). The metabauxite deposits in this zone have a characteristic assemblage of corundum, calcite, margarite, and chloritoid at the marble-metabauxite contact (Jansen & Schuiling, 1976). Feenstra (1985) reports the middle of zone III as the first occurrence of magnetite in the Fe-Ti oxide assemblages, which contradicts Jansen and Schuiling (1976) who report the middle of zone II as the hematite-magnetite transition.

The staurolite-in isograd marks the beginning of zone IV, the corundum-staurolite zone, and is based on the first appearance of Fe-rich staurolite in the metabauxites and pelites (Feenstra, 1996; Feenstra & Wunder, 2002). It was originally mapped as the chloritoid-out isograd based on the disappearance of chloritoid in the pelites and metabauxites (Jansen & Schuiling, 1976), but Feenstra (1985) found chloritoid persisted in a few of the zone IV metabauxites. As the disappearance of chloritoid corresponds to the appearance of staurolite, the first metabauxite staurolite may have formed by the reaction of chloritoid and rutile to form staurolite, chlorite, corundum, ilmenite, and water (Feenstra, 1985). The isograd was originally mapped based on 10 observations of the disappearance of chloritoid in the pelites and metabauxites; it does not appear to have changed in position when it was redefined as the staurolite-in isograd. On Naxos, this reaction occurs at ~540°C (Feenstra & Wunder, 2002; Jansen & Schuiling, 1976). The characteristic metabauxite assemblage is corundum+kyanite+staurolite+biotite+margarite±anorthite±muscovite+Fe-Ti oxides (Feenstra, 1985). At emery-marble contacts, the assemblage of margarite–anorthite–corundum occurs (Jansen & Schuiling, 1976) along with calcite (this study).

The next isograd, sillimanite-in, marks the beginning of zone V and is based on the first appearance of sillimanite in metapelites. On Naxos, at pressures of 6–7 kbar, this occurs at ~620°C (Buick, 1988; Jansen & Schuiling, 1976; Rye, Schuiling, Rye, & Jansen, 1976). Zone V is the kyanite-sillimanite transition zone. Metabauxite deposits are rare in this zone, but generally have the same mineralogy as metabauxites from zone IV; at the metabauxite-marble contacts, the assemblage is anorthite–calcite–corundum (Jansen & Schuiling, 1976). Zone V was previously subdivided into A/B based on the disappearance of kyanite, but this was not supported by the work of Buick (1988) and was removed from later maps (Baker & Matthews, 1994) so zones V-A and V-B are not included in Figure 1.

The melt-in isograd, or migmatite limit, is mapped based on the beginning of partial melting in the pelitic gneisses (660–690°C, Jansen & Schuiling, 1976). The migmatite dome (zone VI) reached the highest metamorphic grade, with pressures of 7–8 kbar and temperatures ~700°C (Buick, 1988; Buick & Holland, 1989; Katzir, Avigad, Matthews, Garfunkel, & Evans, 1999; Katzir, Valley, & Matthews, 2002).

Samples were collected during several field excursions by Valley (in 1996), Katzir (in 2000 and 2003) and Turnier (in 2016) from the metabauxite emery deposits marked with triangles on Figure 1 (extra localities and GPS in Table S3.1 are shown in Figure S3.2 in Appendix S3). These samples are from zones II and IV, and span a range of temperatures, from ~420–600°C (zone II avg. = 424°C, $n = 2$ samples; zone IV avg. = 575°C, $n = 6$ samples; see section 4.1 for a discussion of isograd temperatures). Sample localities, mineral assemblages, and a summary of oxygen isotope results are

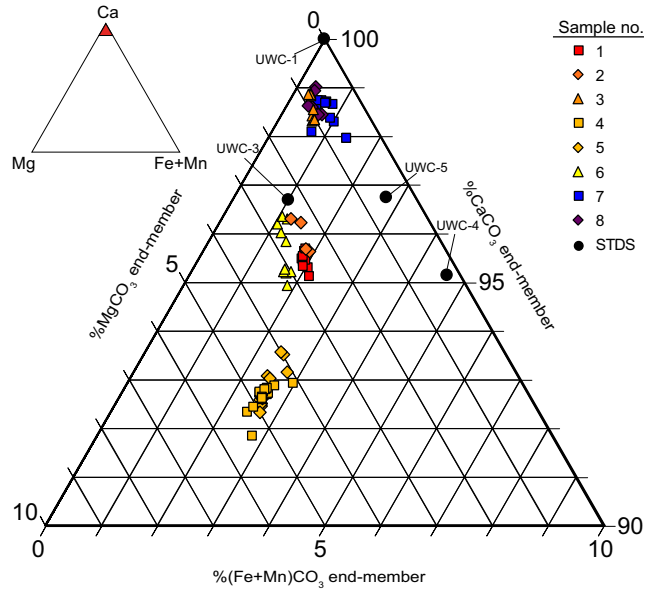

FIGURE 6 Ternary diagram showing carbonate mol % compositions (Ca-Mg-Fe + Mn) for calcite samples 1–8 and four SIMS standards (UWC-1, -3 to -5) determined by EPMA (note: the other standards fall outside of the scaled compositional range shown here). Inset of full ternary is in upper left corner. Red triangle denotes location of larger ternary, for which axes are scaled to highlight the range of carbonate compositions from this study

presented in Table 1 and the modal abundance of minerals in each sample are shown in Table 2.

3 | METHODS

Rocks collected from Naxos were cut into ~2.5 cm chips. After flattening one face, chips were cast into 2.54 cm round epoxy mounts (Figure S3.1 in Appendix S3) to fit within the SIMS sample holder for analysis. Holes for standards (1 mm dia.) were drilled in the middle of the epoxy-held rock chip, then standards UWCrn9 (corundum) and UWC-3 (calcite) were top mounted with epoxy in the holes. The samples were polished progressively from 6 to 1 μm with diamond suspensions and a final polish of 0.05 μm with colloidal alumina. The mounts were then gently cleaned by rinsing with alkaline soap and swirling with ethanol in a beaker. To remove adsorbed water, the sample was first dried with a blast of nitrogen gas and then placed in a vacuum oven at 40°C for at least 3 hr before carbon coating for imaging.

3.1 | Scanning electron microscope

Samples were imaged with a Hitachi S-3400N variable pressure scanning electron microscope (SEM) in the Ray and Mary Wilcox SEM Laboratory at UW-Madison using backscattered electron (BSE), secondary electron (SE), and cathodoluminescence (CL) detectors. Mineral identification was aided by energy-dispersive spectrometry (EDS). Samples were coated with 4–5 nm of carbon for CL imaging. A 20 nm carbon coat was used for BSE, SE, and post-SIMS imaging. Images and EDS were acquired under high vacuum. The EDS system consists of a Si(Li) detector and thin-film window to allow detection of light elements down to carbon. BSE and SE images were mostly made with a 15 kV accelerating voltage, 50–70 nA current, and a working distance of 10 mm; these settings were sometimes varied slightly to optimize the image. CL images were collected using a Gatan PanaCL/F detector with the blue filter inserted to remove streaking from carbonate luminescence (Reed & Milliken, 2003).

3.2 | Electron probe microanalysis

Electron probe microanalysis (EPMA) was performed with a CAMECA SX51 electron microprobe in the Eugene N. Cameron Microscopy and Microanalysis Laboratory at UW-Madison with Probe for EPMA software v. 9.6.4 (Donovan, Kremser, Fournelle, & Goemann, 2018). Calcite was analysed for Mg, Ca, Mn, and Fe. Four WDS spectrometers were used to perform the measurements: a TAP monochromator crystal (2d spacing = 25.745 Å; Mg Kα), two PET crystals (2d = 8.75 Å; Ca Kα and Mn Kα), and a LiF crystal (2d = 4.0267 Å; Fe Kα). Oxygen and carbon were determined by stoichiometry. Samples were coated with a 20 nm carbon coat and at least three EPMA spots were placed around each SIMS calcite pit to obtain enough counts for statistics to optimize precision for trace and minor elements (Fe, Mn, and Mg) while maintaining a low dwell time to minimize specimen damage. The beam diameter was ~5 μm with a 15-kV accelerating voltage and 20-nA beam current.

Peak count times were 120 s for minor elements (Mg, Mn, and Fe) and 12 s for Ca. Standards used were dolomite (Mg), calcite (Ca), rhodochrosite (Mn), and siderite (Fe). A Time Dependent Intensity (TDI) correction procedure was used to determine peak intensities due to specimen damage in calcite. Initially, on- and off-peak counts were used to determine background (sample mounts 2, 4, and 6). Background was counted for 60 s for minor elements and 6 s for Ca. Later, to reduce the analysis time, the Mean Atomic Number (MAN) correction procedure was used to determine background (sample mounts 1, 3, 5, 6, 7, and 8). Phi-rho-z matrix correction (Pouchou & Pichoir, 1991) was used to calculate compositions from k-ratios. Compositions with analytical totals lower than 98% or greater than 102% were excluded (avg. total = 99.5%, $n = 345$).

3.3 | Corundum standard development

The SIMS analysis of $\delta^{18}O$ requires matrix- and chemistry-matched comparison standards (Eiler, Graham, & Valley, 1997; Hervig, Williams, Thomas, Schauer, & Steele, 1992;

Valley & Kita, 2009). Standards must be homogeneous in $\delta^{18}O$ and chemical composition, and be available in sufficient quantity to calibrate by conventional gas-source mass spectrometry. A total of 10 natural and synthetic gem corundum samples were examined. UWCrn9 is the most homogeneous sample in $\delta^{18}O$ by SIMS (±0.29‰ 2SD; Table S3) and was analysed five times by laser fluorination/gas source mass spectrometry to calibrate its $\delta^{18}O$ value (4.94 ± 0.10‰ avg. 2SD VSMOW, Vienna Standard Mean Ocean Water). UWCrn9 was mounted in every sample and used as a running standard for all corundum analyses to correct for any SIMS instrument drift and calibrate the measurements with respect to VSMOW. Details of standard development can be found in Appendix S2.

3.4 | Secondary ion mass spectrometry

Secondary Ion Mass Spectrometry measurements of $\delta^{18}O$ were made in the WiscSIMS Lab (Wisconsin Secondary Ion Mass Spectrometry), Department of Geoscience, UW-Madison, on a CAMECA IMS 1280 ion microprobe. Measurements were conducted with a primary beam of $^{133}Cs^+$, 10 kV accelerating voltage, 20 kV total impact potential, ~2 nA sample current, and 10 μm diameter spot size (1–2 μm deep). Three Faraday cups were used to measure $^{16}O^-$, $^{18}O^-$ and $^{16}OH^-$. Tuning parameters are described by Śliwiński et al. (2016) for calcite and Valley and Kita (2009) for corundum. Typical $^{16}O^-$ count rates were 2.5×10^9 counts per second (cps) for corundum (~2 nA primary beam) and 2×10^9 cps for calcite (~1 nA primary beam).

The analytical standards used to calibrate raw SIMS $\delta^{18}O$ measurements onto the VSMOW scale were UWC-3 for calcite (Kozdon, Ushikubo, Kita, Spicuzza, & Valley, 2009) and UWCrn9 for corundum (Appendix S2). To evaluate any instrument drift, four standard analyses were acquired before and after each bracketed group of 10 unknown analyses. Analytical precision was determined from the 2SD of bracketing standard analyses. The average precision (2SD) is ±0.25‰ for calcite measurements (max = 0.45‰, sample 6) and ±0.26‰ for corundum (max = 0.51‰, sample 2; Table S3.2 in Appendix S3). When propagating analytical precision to the fractionation, the standard deviation of each paired calcite and corundum measurement was added in quadrature (range of propagated 2SD = 0.30 to 0.59‰). After SIMS analysis, pits in both samples and standards were examined by SEM to confirm that cracks, other minerals, and μm-scale inclusions were avoided.

Raw $\delta^{18}O$ values measured in calcite were corrected for matrix effects due to differences in the amounts of Fe, Mn, and Mg measured in samples versus standard. While corrections in this study were minor (i.e. avg. = 0.45‰, max = 1.2‰; Figure S3.12 in Appendix S3), a difference of 5 mol% $MgCO_3$ would change SIMS bias (or instrumental mass fractionation, IMF) by ~0.5‰ (Valley & Kita, 2009). Likewise, matrix effects due to Mg-Fe substitution in dolomite are significant (Śliwiński et al., 2016), and Ca-Fe and Ca-Mn might be significant in calcite. In this study, bias* corrections refer to $\delta^{18}O$ bias values for standards that have been normalized with respect to UWC-1 (end-member calcite) for minor element corrections.

To correct for bias*, calcite standards of varying minor element composition were analysed during each carbonate SIMS session (Turnier, 2017; Appendix A5). Using this suite of calcite standards, the $\delta^{18}O$ values of individual calcite SIMS analyses were corrected using sample compositions obtained by EPMA (Table S5). The procedure for these corrections is summarized in Appendix S4. The bias effects are relatively small because the bias for Ca-Mg is opposite in sign and partly counteracts the bias for Ca-Fe and Ca-Mn. For the Naxos samples, the minor element compositions of calcite within each sample cluster with respect to Fe, Mn, Mg, and Ca (Figure 6). Low-temperature samples 7 and 8 have the lowest amounts of Fe, Mn, and Mg. In this study, differences are minimal between standardization with UWC-3 only versus complex standardization with a range of carbonates (average = 0.45‰). Corrections are greatest for calcite with larger amounts of Fe (Figure S3.12 in Appendix S3).

For an empirical calibration of the calcite-corundum A-factor, it is necessary to obtain values of fractionation for minerals that preserve peak metamorphic equilibrium at the scale of analysis, so SIMS analyses of calcite and corundum are placed as close together as possible while avoiding cracks and inclusions. These are referred to as 'close pairs' of calcite and corundum. Typically, close pairs were less than 100 μm apart. The within-sample fractionations are evaluated for consistency—if representative of equilibrated pairs, fractionation should not vary by more than ~0.6‰ within a single sample that preserves peak metamorphic calcite-corundum isotope fractionation. The limit of 0.6‰ was defined as the 3SD of propagated analytical precision for fractionation values. Variability outside of this limit could be due to effects such as incomplete equilibration or retrogression.

In this study, fractionation consistency is statistically represented by the 2SD of fractionation (Δ(Cc-Crn)) values, which includes any real variability within the samples. This is not the same as the propagated analytical precision for fractionation, which is based on analysis of homogeneous standards. The 2SD of Δ(Cc-Crn) is determined by the standard deviation of within-sample fractionations; it is calculated for each sample based on the number of analyses and deviation of each value from the mean. This is summarized in Table 1 for each sample.

4 | RESULTS

Data from this study are summarized in Table 1. Details are given for mineralogy and modal abundances (Table 2), CL and

BSE images (Figures 2–5), and any isotopic variability (Figures 2 and 5). All bulk and SIMS data are found in the appendix (Tables S1, S2, and S4) and a tabulation of each paired set of calcite and corundum measurements used to determine fractionation are in Table S3.2. Representative paired BSE and CL images for samples that are not shown in the main text are included in the appendix (Figures S3.3 to S3.9 in Appendix S3).

4.1 | Isograds and estimation of temperature

Peak metamorphic temperature for each sample was approximated by linear interpolation of metamorphic gradients between isograds. Isograd temperatures were compared with oxygen isotope fractionations for quartz-kyanite pairs that satisfy the requirements for RAM thermometry in bi-mineral metamorphic veins in M2 pelites on Naxos (Putlitz et al., 2002). Quartz-kyanite pairs from zone IV near the sillimanite-in isograd and zone V yielded temperatures of 635–690°C that match well with estimates from mineral isograds (620–700°C for zone V; Δ(Qz-Ky) from Sharp, 1995). Also, the dehydration of margarite to corundum, anorthite, and water occurs at ~600°C at 5.5 kbar (Rosing, Bird, & Dymek, 1987). The temperature estimated by linear interpolation between isograds for sample 1 (593°C), which contains margarite, corundum, and anorthite, matches well with the temperature at which this dehydration reaction occurs.

Another test of the accuracy of isograd temperatures is by comparison of the carbonate compositions with the calcite-dolomite solvus. None of the calcites in this study are buffered by dolomite and thus the solvus provides only a lower limit for metamorphic temperature. Samples 4 and 5 show the highest Mg content (4.0 to 5.3 mol % $MgCO_3$, Figure 6). Based on the position of the Cc-Dol solvus (Anovitz & Essene, 1987), this composition indicates a temperature greater than 550°C for these rocks. This matches well with the temperature estimates from mineral isograds, which indicate a temperature of ~570°C for these rocks.

4.2 | Mineral identification

Energy-dispersive spectrometry during SEM imaging was used to confirm mineral identification in the polished SIMS mounts for which transmitted light petrography is not possible. The modal mineralogy in samples of this study is presented in Table 2 and agrees with those identified by Feenstra (1985, 1996). Oxidation state was not determined for Fe, so both hematite and magnetite are referred to as 'Fe oxide', and oxides with various proportions of Fe and Ti are called 'Fe-Ti oxides'. For a detailed discussion of oxide and accessory mineralogy of these rocks, refer to Feenstra (1985), who reports magnetite as a major phase in the high-temperature samples (>540°C, zones IV-V) and weakly magnetic Fe-Ti oxides in the low-temperature samples (<540°C, zones I–III; based on reflected-light microscopy and EPMA).

4.3 | Modal abundances

Modal abundances were approximated using ImageJ software and BSE images for areas ~600 × 1,000 μm^2 in dimension. These abundances were used to assess the variation of major minerals at different metamorphic grades and to determine how well the samples approach conditions for RAM thermometry in terms of abundances for minerals with fast and slow rates of oxygen diffusion. The modes are summarized for each sample in Table 2. Areas with representative amounts of major minerals were chosen, but accessory mineral modes are not necessarily representative of the whole sample. In discrete areas, approximately bi-mineral abundances of calcite and corundum are present within a sample that otherwise can have moderate amounts of other minerals when considering a larger domain in the rock.

For samples in this study, mineral modes average 52% calcite, 25% corundum, and 13% or less for other accessory minerals. Oxygen diffuses much more quickly in calcite than in corundum, which is below its closure temperature (Yui et al., 2008) during metamorphism on Naxos. This limits isotopic alteration because retrograde exchange in the rock is dominated by the $\delta^{18}O$ of the fast-diffusing mineral and the slow-diffusing mineral will preserve its isotopic value if it formed below its blocking temperature. Oxygen also diffuses quickly in some of the other minerals, notably muscovite and anorthite (Cole & Chakraborty, 2001; Fortier & Giletti, 1991). Hematite and magnetite are common accessory minerals and inclusions in the corundum, but oxygen diffuses relatively slowly. Overall, the diffusivity rates of oxygen decrease: anorthite>muscovite>calcite>magnetite>hematite>corundum.

Since oxygen diffuses relatively fast in calcite, its potential to exchange oxygen isotopes with other minerals is greater than corundum. Also, calcite in the low-grade rocks is close to its closure temperature (~400°C; Farver, 1994). Using existing data on mineral-calcite fractionation, the isotope fractionation, or $\Delta^{18}O$(Cc-Mineral), calculated for these accessory minerals at 500°C is: 9.9‰ (ΔCc-Mt; Chiba, Chacko, Clayton, & Goldsmith, 1989), 4.6‰ (ΔCc-Mrg; Hoffbauer, Hoernes, & Fiorentini, 1994), 3.5‰ (ΔCc-Msc; Hoffbauer et al., 1994), and 2.7‰ (ΔCc-An; Chiba et al., 1989). Mica is the most abundant mineral after calcite and corundum, and retrograde exchange of mica and calcite would raise the $\delta^{18}O$ value of calcite. The 2SD of Δ(Cc-Crn) values (Table 1) correlates with the mica to calcite ratio (mineral modes, Table 2); samples with higher ratios have greater fractionation variability (samples 2, 4, and 5).

At Naxos, $\delta^{18}O$ variability of calcite (excluding vein calcite) is within 3SD of analytical precision near mica and other

accessory minerals, suggesting minimal diffusion, but this nonetheless could contribute to some of the minor differences in $\delta^{18}O$ measured among calcite from discrete areas with multiple SIMS analyses. Sample 3 has the best modal abundances for RAM thermometry (78% calcite, 9% corundum, 8% tourmaline, 4% mica, and 1% oxides; Table 2) and thus has the least potential for isotopic exchange between calcite and other fast-diffusing minerals. Indeed, sample 3 also has the most consistent values of Δ(Cc-Crn) when comparing fractionations from area-to-area within the same sample (2SD of Δ(Cc-Crn) = 0.33‰; Table 1). Corundum $\delta^{18}O$ is more variable than calcite in most samples, so fractionation variability must be influenced by factors other than oxygen diffusion in calcite.

4.4 | CL textures and isotope zonation

The CL textures in corundum vary among high- and low-grade samples, both among grains within a single sample and among samples crystallized at a similar metamorphic grade. Three main textural types are observed: (a) concentric zoning, (b) mottled zoning, and (c) linear zoning. Concentric zoning occurs as evenly distributed growth domains along the crystallographic faces (Figure 3c). Mottled zoning occurs as patchy zones of varying CL intensity (Figure 4a). Linear zoning appears as lines of different CL intensity cutting across a corundum grain (Figure 4c). These CL textures could have formed by a range of processes, including healed fractures, Ostwald ripening, deformation, growth zoning, or a combination of these processes. Images of zoning are shown for low-grade samples (Figure 3) and for high-grade samples (Figure 4). In general, corundum grains are larger in high-grade samples, but CL textures are variable among samples from a single metamorphic grade.

Despite the variety of CL textures, $\delta^{18}O$ values are consistent in most grains and do not correlate with specific domains of different CL intensity. Dark zones in corundum CL are not systematically different in $\delta^{18}O$ than more brightly luminescing counterparts. The largest isotopic gradients are 1.1‰/60 μm in corundum (Figure 5a) and 0.6‰/150 μm in calcite (Figure 5b). Calcite can sometimes exhibit bright luminescence, but no textural CL zoning was observed in this study. On average, the 2SD of $\delta^{18}O$ for single grains is 0.3‰ for calcite and 0.5‰ for corundum. Within ~500 × 500 μm areas in each sample, the average 2SD of $\delta^{18}O$ values is 0.5‰ for calcite and 0.6‰ for corundum. The larger $\delta^{18}O$ variability in corundum, which is below its closure temperature, could be due to growth zoning. But this is within 3SD of analytical precision and is considered insignificant.

4.5 | Secondary veins and disequilibrium

Fluid flow was limited within the emery pockets on Naxos, as the impermeability of the surrounding marble restricted the migration of externally derived fluids. Instead, fluid in the emery pockets was mostly produced by the dehydration of diaspore to corundum and water (Feenstra & Wunder, 2002). Infrequent calcite veins encountered in low-grade emery are presumed to be secondary because of their fracture-filling textures and variable $\delta^{18}O$ values.

While synmetamorphic veins can contain equilibrated mineral pairs, for example, Putlitz et al. (2002), secondary veins can be texturally and isotopically distinct; often the mineral pairs are not isotopically equilibrated. Figure 7a shows an example of a low-temperature sample (NOA-2-3a) with calcite forming a cross-cutting vein. The analyses from this sample yield large and variable values of fractionation even for close mineral pairs (Δ(Cc-Crn) = 6.3 to 9.9‰, 2SD = 3.2‰). Because vein calcite is not equilibrated with the corundum, these analyses cannot be used in A-factor calibration. By contrast, Figure 8 shows high-temperature sample 1 with much less variable SIMS analyses from calcite and corundum. The values of fractionation are consistent, even among different CL zones in the corundum (avg. Δ(Cc-Crn) = 3.4‰, 2SD = 0.67‰; Table 1).

Most samples contain massive calcite associated with the corundum; three samples (NOA-379, NOA-2-12a and NZ-2-427) contained only vein calcite. These all occurred in the low-grade rocks and were excluded from the thermometry calibration. The other eight samples contained equilibrated assemblages with consistent oxygen isotope fractionation.

5 | DISCUSSION

The SIMS analysis allows avoidance of inclusions and secondary veins. Measurements target mineral pairs that texturally appear to have crystallized at peak metamorphic temperature. Fractionations among close pairs of calcite and corundum, measured by SIMS, have minimal variability. Low-temperature samples have Δ(Cc-Crn) values of 6.3 and 7.2‰ (2SD = 0.91‰); high-temperature samples range from 2.9 to 3.8‰ (2SD = 0.87‰). Values of Δ(Cc-Crn) contrast with the wide range of fractionations calculated from the previous bulk data of high- and low-temperature samples (−2.0 to 6.0‰ and 0.7 to 8.4‰, respectively). Given the variability of vein calcite $\delta^{18}O$ values obtained by SIMS, it is clear that bulk analysis averages peak metamorphic minerals with secondary veins and inclusions in corundum, contributing to the scatter of bulk measurements.

5.1 | Evaluating equilibrium

To examine possible equilibrium versus retrograde exchange, values of $\delta^{18}O(Crn)$ versus $\delta^{18}O(Cc)$ are graphed in Figure 9. Such plots have been used to evaluate equilibrium or determine open-system exchange (Gregory & Criss, 1986). If a group of

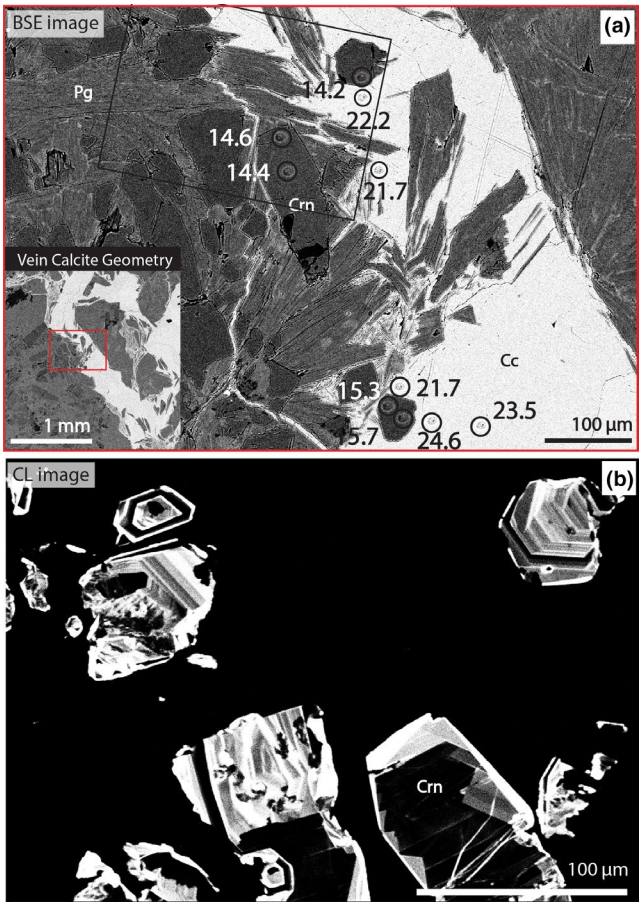

FIGURE 7 Backscattered electrons and cathodoluminescence (CL) images of a low-temperature sample (425°C, NOA-2-3a) with late, vein calcite in emery (Naxos, Greece). SIMS analysis spots and values of $\delta^{18}O$ (VSMOW) are shown in (a). (a) Textural relations of corundum, calcite, and paragonite. The red box in the inset image labelled 'Vein Calcite Geometry' indicates the location of the larger image in (a) and shows the calcite vein. Panel (b) shows a magnified CL image of corundum with oscillatory zoning. The black box in panel (a) shows the location of panel (b). This sample was collected close to sample 7

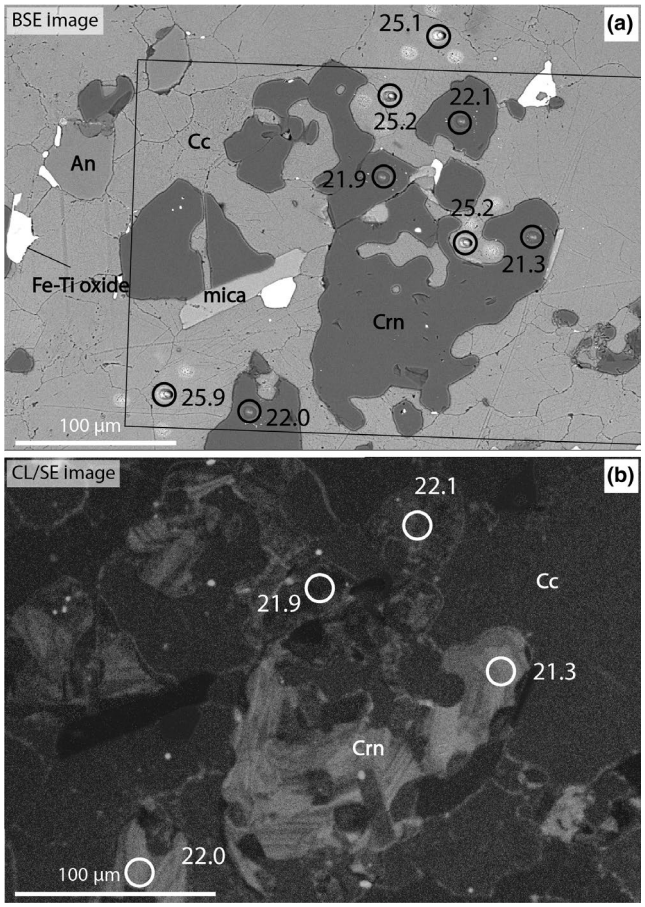

FIGURE 8 CL/SE and backscattered electrons images of sample 1, including SIMS analysis spots (circles) and $\delta^{18}O$ (VSMOW) in calcite and corundum from emery (Naxos, Greece). Black box in (a) shows a portion of the area for the CL image in (b)

rocks has equilibrated at a constant metamorphic temperature, even though the whole-rock $\delta^{18}O$ may be different for each rock, $\delta^{18}O(a)$ versus $\delta^{18}O(b)$ will plot along an isopleth with a slope of one. This is because the value of $\Delta^{18}O(a\text{-}b)$ is constant at a single temperature even though the $\delta^{18}O$ values may differ when the whole-rock values are different.

Thus, analyses from rocks that preserve equilibration at a constant temperature will form a linear array along an isotherm with constant Δ(Cc-Crn). Analyses from rocks preserving a different metamorphic temperature would plot along a different isotherm. These relations allow the evaluation of data quality and whether each sample is consistent with local equilibrium at the peak of metamorphism. Samples that pass this test can be compared with metamorphic temperatures to create an empirical calibration of the A-factor versus temperature. While it is difficult to prove equilibrium, mineral pairs that pass this test are consistent with equilibrium. Alternatively, pairs that do not pass this test are proven to not be equilibrated at the scale of the measurement.

Samples with calcite occurring in veins give erratic and variable values and are not equilibrated at peak metamorphic temperatures. They plot away from the isotherms (Figure S3.10 in Appendix S3) and are not used to calibrate calcite-corundum fractionation. The values of $\delta^{18}O$(Crn) versus $\delta^{18}O$(Cc) for close mineral pairs from the in situ SIMS analyses plot along isotherms for the average temperature of high- and low-grade samples (avg. Δ(Cc-Crn) = 3.3 and 6.8‰, respectively; Figure 9). In detail, individual data points within equilibrated samples will have some scatter, as noted during the previous discussions of isotope zoning, diffusion, and RAM thermometry, but the mean of these data for each sample plots along the isotherms.

5.2 | Disequilibrium effects

Ideal calibration samples will have fractionation variability below 0.6‰, the propagated analytical 3SD of Δ(Cc-Crn). Samples

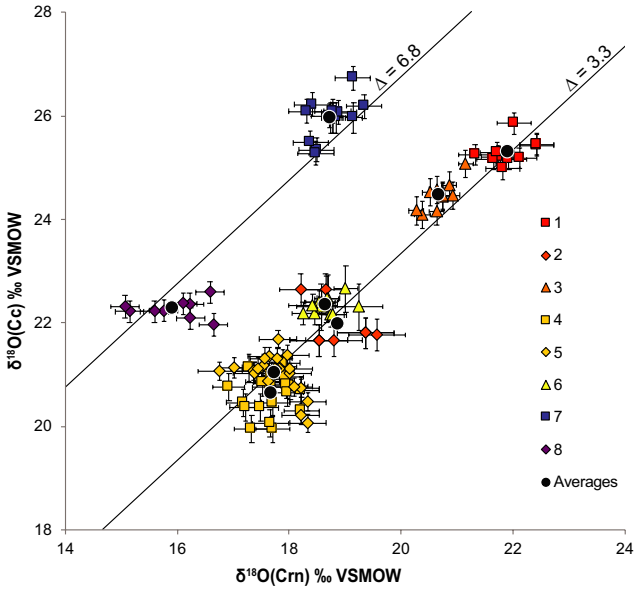

FIGURE 9 Plot of $\delta^{18}O$(Cc) versus $\delta^{18}O$(Crn) measured by SIMS for close pairs of calcite and corundum with isotherms for $\Delta^{18}O$(Cc-Crn) = 6.8 and 3.3‰, the average fractionation for low- and high-temperature samples, respectively. Uncertainty is plotted as 2SD of analytical precision

with variability outside of this are not necessarily excluded but require evaluation. There are several potential causes of variability outside of analytical precision, including retrograde diffusion, secondary mineral generations, and growth zoning.

Secondary mineral generations are highly variable and distinct (2SD = 3.2‰, Figure S3.10 in Appendix S3), but effects from diffusion or growth zoning are more subtle. Oxygen diffuses quickly in calcite, so the potential for calcite $\delta^{18}O$ alteration increases if other minerals with fast oxygen diffusion are locally abundant. These effects appear minimal since the 2SD of calcite $\delta^{18}O$ values is low (range = 0.3 to 0.9‰, avg. = 0.6‰; Table 1) even though the low-grade calcite is near its closure temperature (~400°C). Growth zoning appears to be more abundant in corundum (which is below its closure temperature), although it is not consistent among CL domains. Corundum $\delta^{18}O$ 2SD ranges from 0.5 to 1.2‰ (avg. = 0.7‰; Table 1).

The interplay of effects on calcite and corundum variability within individual samples results in greater 2SD Δ(Cc-Crn) for some samples (sample mounts 2, 3, 4, 5, and 8). Despite this, the self-consistency of fractionation values among rocks from a single grade suggests disequilibrium effects are minor and the main effects on calcite-corundum fractionation are equilibrium processes.

5.3 | Calibration of $\Delta^{18}O$(Cc-Crn)

As discussed above, the $\delta^{18}O$ of fine-grained textures present in these rocks can only be resolved using SIMS analyses in calcite and corundum. Calcite-corundum fractionations calculated from SIMS data yield sample averages that range from 2.93 to 3.77‰ (Table 1) among six different high-grade samples with a similar peak metamorphic temperature. This is reasonable, since linear interpolation between isograds indicates a difference of 25°C among these samples (568 to 593°C). The two low-grade samples have values of 6.33 and 7.20‰ (Table 1) and are from rocks of equivalent metamorphic temperature (~425°C, Table 1).

Measured calcite-corundum fractionations are self-consistent for close pairs within each sample. The 2SE value of fractionation is a good representation of the uncertainty of average fractionation values because it considers the number of analyses; from sample-to-sample, this averages 0.26‰ (range = 0.10 to 0.56‰; Table S4). To determine the A-factor for calcite-corundum fractionation, the average fractionation for each sample (Table 1) is plotted versus the metamorphic temperatures estimated from isograds (1,000 lnα(Cc-Crn) vs. $1/T^2$, Figure 10). In many circumstances, Δ(Cc-Crn), or $\delta^{18}O$(a) - $\delta^{18}O$(b), is a good approximation for 1,000 lnα(*a-b*). For these metamorphic rocks, the differences between 1,000 lnα(Cc-Crn) and Δ(Cc-Crn) range from 0.06 to 0.16‰ (avg. = 0.09‰), which is within analytical precision. The groups of high- and low-temperature samples cluster in 1,000 lnα(Cc-Crn) versus $1/T^2$ space (Figure S3.11 in Appendix S3) and, taken together, define the slope, yielding an A-factor of 2.72 ± 0.34 2SE (Equation 1), assuming 0 fractionation at infinite temperature. The dashed lines in Figure 10 show the boundaries equivalent to ±0.34‰, the 2SE of the linear regression through the origin, and eight data points for sample averages.

The slight non-linearity of the data could indicate a change in slope or more disequilibrium at lower temperatures. For most samples, corundum is more variable than calcite so it could be preserving some growth zoning. Corundum is below its closure temperature, so it is less likely to be affected by retrograde alteration than growth zoning. Another potential factor is the accuracy of the corundum-in isograd temperature. If the isograd temperature is lower, it would shift the fractionation closer to the linear regression.

Despite this, all eight samples are within analytical uncertainty of the linear regression. The median of low-temperature sample 7 plots above the line but is within error. If only the high-temperature data and origin are used to define the slope, a slightly smaller A-factor of 2.36 results, but this value is approximately within error of the linear regression 2SE. The isograd temperatures are estimated to be accurate to ±50°C, providing an additional uncertainty based on the placement of isograds and determination of their temperatures.

The fractionations determined empirically in this study result in a calibration of the 1,000 lnα(Cc-Crn) versus temperature. This is compared with the polynomial curve calculated using the modified increment method (Zheng, 1991,

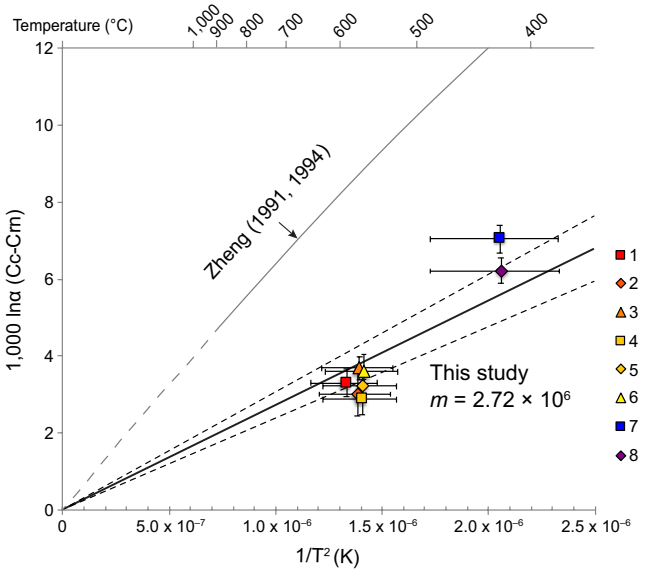

FIGURE 10 Plot of 1,000 lnα(Cc-Crn) versus $1/T^2$ (K) for sample averages. Sample temperatures are based on mineral isograds (Figure 1). *X*-axis error bars are ± 50°C and *y*-axis error bars show propagated analytical 2SD from SIMS data precision. The data from this study yield an A-factor of 2.72. The dashed lines show the upper and lower bounds of the field for A(Cc-Crn) = 2.72 ± 0.3. The calibration curve calculated from mineral-water fractionations using the increment method (Zheng, 1991, 1994) is also shown

1994) in Figure 10. At 1,000 K, the modified increment method derives a fractionation of 6.5‰, which is more than twice the value of 2.7‰ empirically derived in this study. If the modified increment fractionation is applied to the values of Δ^{18}O(Cc-Crn) measured in this study by SIMS, estimated temperatures are unreasonably high when compared with the metamorphic mineral equilibria at Naxos, Greece. The high-temperature samples from zone IV have calculated temperatures of 975–1140°C for rocks collected between the staurolite-in isograd (540°C) and the sillimanite-in isograd (620°C). Furthermore, these temperatures would be significantly above the temperature of partial melting (migmatite limit, ~700°C; Figure 1). As such, the modified increment calibration is not consistent with reasonable metamorphic temperatures and the values of Δ^{18}O(Cc-Crn) measured for close pairs of calcite and corundum.

5.4 | Mineral-corundum A-factors

The empirical calcite-corundum A-factor of this study for oxygen isotope fractionation can be combined with other data to derive a suite of mineral-corundum A-factors (left column, Table 3). The oxygen isotope fractionation of calcite has been calibrated against a range of other minerals by experimental, theoretical, and empirical methods (Chacko et al., 2001; Fallick et al., 2019; O'Neil, Clayton, & Mayeda, 1969; Valley, 2003; Zheng, 1994). These calibrations allow derivation of mineral-corundum A-factors:

$$A\,(a-c)=A\,(a-b)+A\,(b-c)\,, \tag{3}$$

where *a*, *b* and *c* are minerals and *A* is the A-factor for each particular mineral–mineral pair. In the case of this study, mineral *b* is calcite and *c* is corundum, and they can be used to derive A-factors between corundum and other minerals (*a*).

If there are available data for a mineral-calcite system of interest and the linear A-factor approximation is valid (Equation 1), these mineral-calcite A-factors can be used (in Equation 3) to derive the A-factors for other minerals. The matrix of mineral-corundum A-factors in Table 3 is based on calcite–mineral fractionations from Valley (2003) and references therein. Additional spinel-mineral A-factors were calculated from the value of equilibrium Δ^{18}O(Cc-spinel) reported in Fallick et al. (2019; Δ^{18}O(Cc-spinel) = 3.7‰ at T = 620°C) and mineral-corundum A-factors from the current study.

5.5 | Genesis of basalt-hosted sapphire

The A-factor for zircon-corundum (A(Zrc-Crn) = 0.46, Table 3) provides new insight for evaluating corundum genesis. Wong and Verdel (2017) include a catalogue of sapphire δ^{18}O values from different rock types. These data (Figure 11) are from 74 localities among 19 countries, detailing the δ^{18}O variation among gem corundums found in metamorphic, metasomatic, and mafic to ultramafic igneous deposits. The δ^{18}O values range from 1.7 to 19.9‰ (avg. = 6.7‰). Of these data, corundum from metamorphic and metasomatic deposits range from 1.7 to 19.9‰ (avg. = 9.7‰), and corundum associated with mafic to ultramafic deposits range from 2.7 to 13.9‰ (avg. = 5.7‰). Zircons equilibrated at magmatic temperatures with typical mantle have δ^{18}O = 4.7 to 5.9‰ (5.3 ± 0.6‰ 2SD, Valley et al., 2005). Thus, corundum equilibrated with this mantle value will have an average δ^{18}O of 5.1 ± 0.6‰ 2SD at 1,200°C and range from 4.4 to 5.7‰.

This range of values calculated for a primitive mantle-like corundum is shown by a grey bar on a histogram of gem corundum δ^{18}O values (Figure 11). The top histogram shows the distribution in δ^{18}O of corundum associated with mafic and ultramafic rocks (including basalt, lamprophyre, pyroxenite, and basanite), which are plotted together because they have similar δ^{18}O values. Even though the host rocks for corundum are mantle related, the corundum δ^{18}O ranges to higher values than mantle-like corundum, overlapping with δ^{18}O values seen in corundum from metamorphic and metasomatic deposits (bottom histogram, Figure 11). The high-δ^{18}O corundum could not have crystallized from primitive mantle magmas. Furthermore, the textures suggest that the corundum is not in equilibrium with the host magma, making the corundum inherently xenocrystic.

TABLE 3 Selected mineral–mineral A-factors (Equation 1) for oxygen isotopes using the calcite-corundum A-factor (2.72) from this study and fractionation data from Fallick et al. (2019) and Valley (2003), and references therein; mineral abbreviations are as defined in Table 1

Prv	−3.70													
Mt	−3.19	0.51												
Ru	−1.59	2.11	1.60		$\Delta_{a\text{-}b} \approx 1{,}000\ \ln\alpha(a-b) = A(a-\mathrm{b}) \times 10^6\ T^{-2}$									
Fo	−0.57	3.13	2.62	1.02	Where a = Y-axis and b = X-axis mineral									
Ttn	−0.56	3.14	2.63	1.03	0.01									
Sp	−0.23	3.47	2.96	1.36	0.34	0.33								
Gr	0.07	3.77	3.26	1.66	0.64	0.63	0.30							
Di	0.35	4.05	3.54	1.94	0.92	0.91	0.58	0.28						
Alm	0.39	4.09	3.58	1.98	0.96	0.95	0.62	0.32	0.04					
Zrc	0.46	4.16	3.65	2.05	1.03	1.02	0.69	0.39	0.11	0.07				
Ap	0.59	4.29	3.78	2.18	1.16	1.15	0.82	0.52	0.24	0.20	0.13			
An	1.11	4.81	4.30	2.70	1.68	1.67	1.34	1.04	0.76	0.72	0.65	0.52		
Ab	2.16	5.86	5.35	3.75	2.73	2.72	2.39	2.09	1.81	1.77	1.70	1.57	1.05	
Cc	2.72	6.42	5.91	4.31	3.29	3.28	2.95	2.65	2.37	2.33	2.26	2.13	1.61	0.56
	Crn	Prv	Mt	Ru	Fo	Ttn	Sp	Gr	Di	Alm	Zrc	Ap	An	Ab

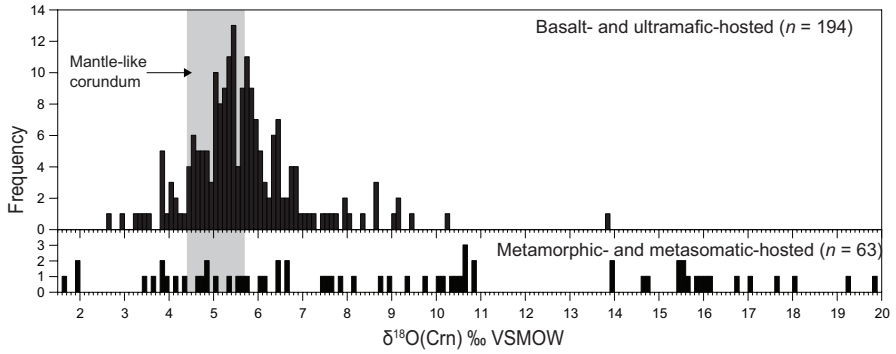

FIGURE 11 Stacked histograms of frequency versus $\delta^{18}O$ (‰) VSMOW showing the global range of oxygen isotope values measured in basalt- and ultramafic-hosted sapphires (top) and metamorphic- and metasomatic-hosted sapphires (bottom). The grey field denotes the range of values predicted for corundum equilibrated with a primitive, mantle-like magma (see text). Sapphire data are from Wong and Verdel (2017) and references therein

Although most of the sapphires plotted in Figure 11 are found in placer deposits, they are thought to originate from nearby rock types (e.g. basalt, lamprophyre, and basanite). Even within a single corundum locality, the $\delta^{18}O$ can be quite variable. Among the localities in Figure 11, placer corundum associated with basalt fields from Madagascar, the French Massif Central, and Thailand are the most variable. The $\delta^{18}O$ value of gem sapphire ranges from 3.9 to 9.5‰ at Vatromandry, Madagascar, 2.7 to 6.9‰ at Antisrabe, Madagascar, 4.7 to 8.4‰ at Denchai, Thailand, and 4.9 to 10.3‰ at Le Mont Coupet, French Massif Central.

The variability within single localities and the overall range of $\delta^{18}O$ indicates that many of these sapphires did not crystallize from primitive mantle-derived melt. Instead, it suggests that sapphire formed from variable protoliths at different stages of melt evolution and crustal contamination. Insights from the application of oxygen isotope equilibrium and thermometry will allow us to better understand the nature and evolution of these enigmatic corundum deposits.

6 | CONCLUSIONS

The emery deposits of Naxos, Greece, provide an excellent opportunity to calibrate the A-factor for close mineral pairs of corundum and calcite by SIMS. The metamorphic isograds mapped in the emery deposits and surrounding pelitic schists provide an independent estimate of peak metamorphic temperature. Previous attempts to assess corundum-calcite fractionation using bulk analyses of mineral concentrates from these rocks were unsuccessful. By contrast, accurate and precise in situ analyses of $\delta^{18}O$ at a spatial resolution of 10 μm yield self-consistent values

and variation in the calcite-corundum fractionations consistent with temperature estimates based on metamorphic isograds. Using SIMS analysis guided by CL and BSE imaging, inclusions in corundum, along with secondary, disequilibrium isotope zones, or late, retrograde minerals and veins, can be avoided. This allows for a consistent value of calcite-corundum fractionation from close mineral pairs to be obtained and interpreted to represent equilibrated peak metamorphic values.

When calibrated against temperature estimates from metamorphic isograds, data from this study yield an empirically determined A-factor of 2.72 ± 0.3 (2SE) for the oxygen isotope fractionation between calcite and corundum. This value (2.72) is significantly smaller than that calculated from previous theoretically determined values (1,000 lnα(Cc-Crn) = 6.5‰ at 1,000 K). Using the new A-factor, crystallization temperatures for corundum in equilibrium with other mineral species can be calculated for a variety of different minerals. In addition, the $\delta^{18}O$ of minerals crystallized in equilibrium can be determined from independent temperature estimates.

The corundum-zircon fractionation was used in conjunction with compositions of zircon from primitive mantle to find the $\delta^{18}O$ range of mantle-like corundum (5.1 ± 0.6‰). Based on the $\delta^{18}O$ range of sapphire hosted in mafic and ultramafic rocks, we propose that many of these sapphires crystallized in association with evolved magmas that interacted with the crust and are thus xenocrystic to the mantle rocks in which they are found.

ACKNOWLEDGEMENTS

We thank Brian Hess for sample preparation, the WiscSIMS group for SIMS support, John Fournelle and Aurélien Moy for EPMA help, Bil Schneider and Phil Gopon for SEM training and aid, Maciej Śliwiński for corrections of SIMS bias for carbonates, and Noriko Kita for SIMS advice. We are grateful to Alan Matthews for helpful discussions and a thoughtful review. We also thank an anonymous reviewer for constructive comments and Donna Whitney for great editorial contributions and suggestions for our manuscript. This work was supported by the National Science Foundation (EAR-1525336). WiscSIMS is supported by NSF (EAR-1355590, 1658823) and UW-Madison. RT received a UW-Madison Advanced Opportunity Fellowship. Fieldwork was aided by the UW Geoscience Department. We declare no conflict of interest.

ORCID

Rachelle B. Turnier https://orcid.org/0000-0002-3589-5364
Yaron Katzir https://orcid.org/0000-0003-1999-3746
Kouki Kitajima https://orcid.org/0000-0001-7634-4924
Ian J. Orland https://orcid.org/0000-0002-4853-4111
Michael J. Spicuzza https://orcid.org/0000-0001-8548-3088
John W. Valley https://orcid.org/0000-0003-3530-2722

REFERENCES

Anovitz, L. M., & Essene, E. J. (1987). Phase equilibria in the system $CaCO_3$-$MgCO_3$-$FeCO_3$. *Journal of Petrology*, *28*, 389–415. https://doi.org/10.1093/petrology/28.2.389

Avigad, D. (1998). High-pressure metamorphism and cooling on SE Naxos. *European Journal of Mineralogy*, *10*, 1309–1319. https://doi.org/10.1127/ejm/10/6/1309

Aydoğan, M. S., & Moazzen, M. (2012). Origin and metamorphism of corundum-rich metabauxites at Mt. Ismail in the Southern Menderes Massif, SW Turkey. *Resource Geology*, *62*, 243–262. https://doi.org/10.1111/j.1751-3928.2012.00193.x

Baker, J., & Matthews, A. (1994). Textural and isotopic development of marble assemblages during the Barrovian-style M2 metamorphic event, Naxos, Greece. *Contributions to Mineralogy and Petrology*, *116*, 130–144. https://doi.org/10.1007/BF00310695

Bolhar, R., Ring, U., & Ireland, T. R. (2017). Zircon in amphibolite from Naxos, Aegean Sea, Greece: Origin, significance and tectonic setting. *Journal of Metamorphic Geology*, *35*, 413–434. https://doi.org/10.1111/jmg.12238

Bowman, J. R., Valley, J. W., & Kita, N. T. (2009). Mechanisms of oxygen isotopic exchange and isotopic evolution of $^{18}O/^{16}O$-depleted periclase zone marbles in the Alta aureole, Utah: Insights from ion microprobe analysis of calcite. *Contributions to Mineralogy and Petrology*, *157*, 77–93. https://doi.org/10.1007/s00410-008-0321-1

Buick, I. S. (1988). *The metamorphic and structural evolution of the Barrovian overprint, Naxos, Cyclades, Greece*. Unpublished doctoral dissertation (p. 235). University of Cambridge.

Buick, I. S., & Holland, T. J. B. (1989). The P-T-t path associated with crustal extension, Naxos, Cyclades, Greece. *Geological Society of London Special Publication*, *43*, 365–369. https://doi.org/10.1144/gsl.sp.1989.043.01.32

Chacko, T., Cole, D. R., & Horita, J. (2001). Equilibrium oxygen, hydrogen and carbon isotope fractionation factors applicable to geologic systems. *Reviews in Mineralogy and Geochemistry*, *43*, 1–81. https://doi.org/10.2138/gsrmg.43.1.1

Chiba, H., Chacko, T., Clayton, R. N., & Goldsmith, J. R. (1989). Oxygen isotope fractionations involving diopside, forsterite, magnetite, and calcite: Application to geothermometry. *Geochimica et Cosmochimica Acta*, *53*, 2985–2995. https://doi.org/10.1016/0016-7037(89)90174-9

Cole, D. R., & Chakraborty, S. (2001). Rates and Mechanisms of Isotopic Exchange. *Reviews in Mineralogy and Geochemistry*, *43*, 83–223. https://doi.org/10.2138/gsrmg.43.1.83

Donovan, J., Kremser, D., Fournelle, J., & Goemann, K. (2018). *Probe for Windows User's Guide and Reference*, *Enterprise Edition* (p. 431). Eugene, OR: Probe Software Inc.

Duchêne, S., Aïssa, R., & Vanderhaeghe, O. (2006). Pressure-temperature-time evolution of metamorphic rocks from Naxos (Cyclades, Greece): Constraints from thermobarometry and Rb/Sr

dating. *Geodinamica Acta*, *19*(5), 301–321. https://doi.org/10.3166/ga.19.301-321

Eiler, J. M., Baumgartner, L. P., & Valley, J. W. (1992). Intercrystalline stable isotope diffusion: A fast grain boundary model. *Contributions to Mineralogy and Petrology*, *112*, 543–557. https://doi.org/10.1007/BF00310783

Eiler, J. M., Graham, C., & Valley, J. W. (1997). SIMS analysis of oxygen isotopes: Matrix effects in complex minerals and glasses. *Chemical Geology*, *138*, 221–244. https://doi.org/10.1016/S0009-2541(97)00015-6

Eiler, J. M., Valley, J. W., & Baumgartner, L. P. (1993). A new look at stable isotope thermometry. *Geochimica et Cosmochimica Acta*, *57*, 2571–2583. https://doi.org/10.1016/0016-7037(93)90418-V

Errico, J. C., Barnes, J. D., Strickland, A., & Valley, J. W. (2013). Oxygen isotope zoning in garnets from Franciscan eclogite blocks: Evidence for rock–buffered fluid interaction in the mantle wedge. *Contributions to Mineralogy and Petrology*, *166*, 1161–1176. https://doi.org/10.1007/s00410-013-0915-0

Fallick, A., Giuliani, G., Rigaudier, T., Boyce, A. J., Long Pham, V., & Pardieu, V. (2019). Remarkably uniform oxygen isotope systematics for co-existing pairs of gem-spinel and calcite in marble, with special reference to Vietnamese deposits. *Comptes Rendus Geoscience*, *351*, 27–36. https://doi.org/10.1016/j.crte.2018.11.008

Farver, J. R. (1994). Oxygen self-diffusion in calcite: Dependence on temperature and water fugacity. *Earth and Planetary Science Letters*, *121*, 575–587. https://doi.org/10.1016/0012-821X(94)90092-2

Feenstra, A. (1985). Metamorphism of bauxites on Naxos, Greece. *Geologica Ultraiectina*, *39*, 1–206.

Feenstra, A. (1996). An EMP and TEM—AEM study of margarite, muscovite and paragonite in polymetamorphic metabauxites of Naxos (Cyclades, Greece) and the implications of fine-scale mica interlayering and multiple mica generations. *Journal of Petrology*, *37*, 201–233. https://doi.org/10.1093/petrology/37.2.201

Feenstra, A., & Wunder, B. (2002). Dehydration of diasporite to corundite in nature and experiment. *Geology*, *30*, 119–122. https://doi.org/10.1130/0091-7613(2002)030<0119:DODTCI>2.0.CO;2

Ferry, J. M., Kitajima, K., Strickland, A., & Valley, J. W. (2014). Ion microprobe survey of the grain-scale oxygen isotope geochemistry of minerals in metamorphic rocks. *Geochimica et Cosmochimica Acta*, *144*, 403–433. https://doi.org/10.1016/j.gca.2014.08.021

Ferry, J. M., Ushikubo, T., Kita, N. T., & Valley, J. W. (2010). Assessment of grain-scale homogeneity and equilibration of carbon and oxygen isotope compositions of minerals in carbonate-bearing metamorphic rocks by ion microprobe. *Geochimica et Cosmochimica Acta*, *74*, 6517–6540. https://doi.org/10.1016/j.gca.2010.08.039

Fortier, S. M., & Giletti, B. J. (1991). Volume self-diffusion of oxygen in biotite, muscovite, and phlogopite micas. *Geochimica et Cosmochimica Acta*, *55*, 1319–1330. https://doi.org/10.1016/0016-7037(91)90310-2

Giuliani, G., Ohnenstetter, D., Fallick, A. E., Groat, L. A., & Fagan, A. J. (2014). The geology and genesis of gem corundum deposits. *Mineralogical Association of Canada Short Course*, *44*, 23–112.

Gordon, S. M., Luffi, P., Hacker, B., Valley, J., Spicuzza, M., Kozdon, R., … Minaev, V. (2012). The thermal structure of continental crust in active orogens: Insight from Miocene eclogite and granulite xenoliths of the Pamir Mountains. *Journal of Metamorphic Geology*, *30*, 413–434. https://doi.org/10.1111/j.1525-1314.2012.00973.x

Gregory, R. T., & Criss, R. E. (1986). Isotopic exchange in open and closed systems. *Reviews in Mineralogy*, *16*, 91–127.

Hervig, R. L., Williams, P., Thomas, R. M., Schauer, S. N., & Steele, I. M. (1992). Microanalysis of oxygen isotopes in insulators by secondary ion mass spectrometry. *International Journal of Mass Spectrometry and Ion Processes*, *120*, 45–63. https://doi.org/10.1016/0168-1176(92)80051-2

Hoefs, J. (2018). *Stable isotope geochemistry* (p. 437). New York, NY: Springer International Publishing.

Hoffbauer, R., Hoernes, S., & Fiorentini, E. (1994). Oxygen isotope thermometry based on a refined increment method and its application to granulite-grade rocks from Sri Lanka. *Precambrian Research*, *66*, 199–220. https://doi.org/10.1016/0301-9268(94)90051-5

Jansen, J. B. H. (1977). *The Geology of Naxos* (Vol 19, p. 100). Athens: Institute of geological and mining research.

Jansen, J. B. H., & Schuiling, R. D. (1976). Metamorphism on Naxos; petrology and geothermal gradients. *American Journal of Science*, *276*, 1225–1253. https://doi.org/10.2475/ajs.276.10.1225

Katzir, Y., Avigad, D., Matthews, A., Garfunkel, Z., & Evans, B. W. (1999). Origin and metamorphism of ultrabasic rocks associated with a subducted continental margin, Naxos (Cyclades, Greece). *Journal of Metamorphic Geology*, *17*, 301–318. https://doi.org/10.1046/j.1525-1314.1999.00197.x

Katzir, Y., & Valley, J. W. (2001). Calcite-corundum oxygen isotope fractionations in Naxos metabauxites; selecting samples for thermometry. Geological Society of America, Annual Meeting Abstract, #25470.

Katzir, Y., Valley, J. W., Matthews, A., & Spicuzza, M. J. (2002). Tracking fluid flow during deep crustal anatexis: Metasomatism of peridotites (Naxos, Greece). *Contributions to Mineralogy and Petrology*, *142*, 700–713. https://doi.org/10.1007/s00410-001-0319-4

Keay, S., Lister, G., & Buick, I. S. (2001). The timing of partial melting, Barrovian metamorphism and granite intrusion in the Naxos metamorphic core complex, Cyclades, Aegean Sea, Greece. *Tectonophysics*, *342*, 275–312. https://doi.org/10.1016/S0040-1951(01)00168-8

Kitchen, N. E., & Valley, J. W. (1995). Carbon isotope thermometry in marbles of the Adirondack Mountains, New York. *Journal of Metamorphic Geology*, *13*, 577–594. https://doi.org/10.1111/j.1525-1314.1995.tb00244.x

Kozdon, R., Ushikubo, T., Kita, N. T., Spicuzza, M., & Valley, J. W. (2009). Intratest oxygen isotope variability in the planktonic foraminifer N. pachyderma: Real vs. apparent vital effects by ion microprobe. *Chemical Geology*, *258*, 327–337. https://doi.org/10.1016/j.chemgeo.2008.10.032

Martin, L., Duchéne, S., Deloule, E., & Vanderheaghe, O. (2006). The isotopic composition of zircon and garnet: A record of the metamorphic history of Naxos, Greece. *Lithos*, *87*, 174–192. https://doi.org/10.1016/j.lithos.2005.06.016

O'Neil, J. R. (1986). Theoretical and experimental aspects of isotopic fractionation. *Reviews in Mineralogy*, *16*, 1–40.

O'Neil, J. R., Clayton, R. N., & Mayeda, T. K. (1969). Oxygen isotope fractionation in divalent metal carbonates. *Journal of Chemical Physics*, *51*, 5547–5558. https://doi.org/10.1063/1.1671982

Page, F. Z., Essene, E. J., Mukasa, S. B., & Valley, J. W. (2014). A garnet–zircon oxygen isotope record of subduction and exhumation fluids from the Franciscan Complex, California. *Journal of Petrology*, *55*, 103–131. https://doi.org/10.1093/petrology/egt062

Pouchou, J. L., & Pichoir, F. (1991). Quantitative analysis of homogenous or stratified microvolumes applying the model "PAP". In *Electron probe quantitation* (pp. 31–75). New York, NY: Plenum Press.

Putlitz, B., Valley, J. W., Matthews, A., & Katzir, Y. (2002). Oxygen isotope thermometry of quartz–Al_2SiO_5 veins in high-grade metamorphic rocks on Naxos island (Greece). *Contributions to Mineralogy and Petrology*, *143*, 350–359. https://doi.org/10.1007/s00410-002-0346-9

Quinn, R. J., Kitajima, K., Nakashima, D., Spicuzza, M. J., & Valley, J. W. (2017). Oxygen isotope thermometry using quartz inclusions in garnet. *Journal of Metamorphic Geology*, *35*, 231–252. https://doi.org/10.1111/jmg.12230

Reed, R. M., & Milliken, K. L. (2003). How to overcome imaging problems associated with carbonate minerals on SEM-based cathodoluminescence systems. *Journal of Sedimentary Research*, *73*, 328–332. https://doi.org/10.1306/081002730328

Rosing, M. T., Bird, D. K., & Dymek, R. F. (1987). Hydration of corundum-bearing xenoliths in the Qôrqut Granite Complex, Godthåbsfjord, West Greenland. *American Mineralogist*, *72*, 29–38.

Russell, A. K., Kitajima, K., Strickland, A., Medaris, L. G., Schulze, D. J., & Valley, J. W. (2013). Eclogite-facies fluid infiltration: Constraints from $\delta^{18}O$ zoning in garnet. *Contributions to Mineralogy and Petrology*, *165*, 103–116. https://doi.org/10.1007/s00410-012-0794-9

Rye, R. O., Schuiling, R. D., Rye, D. M., & Jansen, J. B. H. (1976). Carbon, hydrogen, and oxygen isotope studies of the regional metamorphic complex at Naxos, Greece. *Geochimica et Cosmochimica Acta*, *40*, 1031–1049. https://doi.org/10.1016/0016-7037(76)90045-4

Schuiling, R. D., & Oosterom, M. G. (1967). The metamorphic complex on Naxos (Greece) and the strontium and barium content of its carbonate rocks. *Proceedings of the Koninklijke Nederlandse Akademie van Wetenschappen*, *70*(2), 165–175.

Sharp, Z. D. (1995). Oxygen isotope geochemistry of the Al_2SiO_5 polymorphs. *American Journal of Science*, *295*, 1058–1076. https://doi.org/10.2475/ajs.295.9.1058

Śliwiński, M. G., Kitajima, K., Kozdon, R., Spicuzza, M. J., Fournelle, J. H., Denny, A., & Valley, J. W. (2016). Secondary ion mass spectrometry bias on isotope ratios in dolomite–ankerite, Part I: $\delta^{18}O$ Matrix Effects. *Geostandards and Geoanalytical Research*, *40*, 157–172. https://doi.org/10.1111/j.1751-908x.2015.00364.x

Turnier, R. B. (2017). *Calibration of oxygen isotope fractionation and corundum-calcite thermometry in emery at Naxos, Greece*. In Situ Versus Bulk Analysis. *Unpublished M.S. Thesis* (p. 53). University of Wisconsin-Madison.

Valley, J. W. (2001). Stable isotope thermometry at high temperatures. *Reviews in Mineralogy and Geochemistry*, *43*, 365–413. https://doi.org/10.2138/gsrmg.43.1.365

Valley, J. W. (2003). Oxygen isotopes in zircon. *Reviews in Mineralogy and Geochemistry*, *53*, 343–385. https://doi.org/10.2113/0530343

Valley, J. W., & Kita, N. T. (2009). In situ oxygen isotope geochemistry by ion microprobe. *Mineralogical Association of Canada Short Course*, *41*, 19–63.

Valley, J. W., Lackey, J. S., Cavosie, A. J., Clechenko, C. C., Spicuzza, M. J., Basei, M. A. S., … Wei, C. S. (2005). 4.4 billion years of crustal maturation: Oxygen isotope ratios of magmatic zircon. *Contributions to Mineralogy and Petrology*, *150*, 561–580. https://doi.org/10.1007/s00410-005-0025-8

Vielzeuf, D., Champenois, M., Valley, J. W., Brunet, F., & Devidal, J. L. (2005). SIMS analyses of oxygen isotopes: Matrix effects in Fe–Mg–Ca garnets. *Chemical Geology*, *223*, 208–226. https://doi.org/10.1016/j.chemgeo.2005.07.008

Voudouris, P., Mavrogonatos, C., Graham, I., Giuliani, G., Melfos, V., Karampelas, S., … Lampridis, A. (2019). Gem corundum deposits of Greece: Geology, mineralogy and genesis. *Minerals*, *9*(1), 49. https://doi.org/10.3390/min9010049

Wijbrans, J. R., & McDougall, I. (1988). Metamorphic evolution of the Attic-Cycladic metamorphic belt on Naxos (Cyclades, Greece) utilizing $^{40}Ar/^{39}Ar$ age spectrum measurements. *Journal of Metamorphic Geology*, *6*, 571–594. https://doi.org/10.1111/j.1525-1314.1988.tb00441.x

Wong, J., & Verdel, C. (2017). Tectonic environments of sapphire and ruby revealed by a global oxygen isotope compilation. *International Geology Review*, *60*(2), 188–195. https://doi.org/10.1080/00206814.2017.1327373

Yui, T.-F., Zaw, K., & Wu, C.-M. (2008). A preliminary stable isotope study on Mogok Ruby, Myanmar. *Ore Geology Reviews*, *34*, 192–199. https://doi.org/10.1016/j.oregeorev.2008.05.001

Zheng, Y.-F. (1991). Calculation of oxygen isotope fractionation in metal oxides. *Geochimica et Cosmochimica Acta*, *55*, 2299–2307. https://doi.org/10.1016/0016-7037(91)90105-E

Zheng, Y.-F. (1994). Oxygen isotope fractionation in metal monoxides. *Mineralogical Magazine*, *58A*, 1000–1001.

SUPPORTING INFORMATION

Additional supporting information may be found online in the Supporting Information section.

Table S1. Bulk Naxos $\delta^{18}O$ corundum LF data.

Table S2. Bulk Naxos $\delta^{18}O$ acid dissolution calcite data.

Table S3. Catalogue of all standard development SIMS data.

Table S4. Catalogue of all Naxos A-factor calibration SIMS data. Discarded analyses are denoted with grey font and justified in the 'comments' column.

Table S5. Catalogue of all Naxos calcite EPMA data for composition bias correction.

Appendix S1. Tabulated Bulk Fractionation.

Appendix S2. Corundum Standard Development.

Appendix S3. Naxos SIMS Supplementary Material.

Appendix S4. SIMS Carbonate Composition Bias Correction.

How to cite this article: Turnier RB, Katzir Y, Kitajima K, Orland IJ, Spicuzza MJ, Valley JW. Calibration of oxygen isotope fractionation and calcite-corundum thermometry in emery at Naxos, Greece. *J Metamorph Geol*. 2020;38:53–70. https://doi.org/10.1111/jmg.12512